

**Supporting information for:**

**Improved Alchemical Free Energy Calculations with  
Optimized Smoothstep Softcore Potentials**

Tai-Sung Lee,<sup>†</sup> Zhixiong Lin,<sup>‡</sup> Bryce K. Allen,<sup>‡</sup> Charles Lin,<sup>‡</sup> Brian K. Radak,<sup>‡</sup>  
Yujun Tao,<sup>†</sup> Hsu-Chun Tsai,<sup>†</sup> Woody Sherman,<sup>‡</sup> and Darrin M. York<sup>\*,†</sup>

*Laboratory for Biomolecular Simulation Research, Institute for Quantitative Biomedicine  
and Department of Chemistry and Chemical Biology, Rutgers University, Piscataway, NJ  
08854, USA , and Silicon Therapeutics LLC, Boston, MA 02111, USA*

E-mail: [Darrin.York@rutgers.edu](mailto:Darrin.York@rutgers.edu)

---

\*To whom correspondence should be addressed

<sup>†</sup>Laboratory for Biomolecular Simulation Research, Institute for Quantitative Biomedicine and Department of Chemistry and Chemical Biology, Rutgers University, Piscataway, NJ 08854, USA

<sup>‡</sup>Silicon Therapeutics LLC, Boston, MA 02111, USA

# Contents

|          |  |            |
|----------|--|------------|
| <b>1</b> | <b>The direct space implementation of the electrostatic interaction</b>  | <b>S2</b>  |
| <b>2</b> | <b>Simulation setup and protocols</b>  | <b>S4</b>  |
| 2.1      | Three representative model systems . . . . .   | S5         |
| 2.2      | Hydration free energies . . . . .  | S6         |
| 2.3      | The Wang, <i>et al.</i> dataset . . . . .  | S6         |
| <b>3</b> | <b>Representative <math>\langle \frac{\partial U}{\partial \lambda} \rangle_\lambda</math> curves</b>                                | <b>S8</b>  |
| <b>4</b> | <b>The smooth step functions of different orders and their derivatives:</b>  | <b>S11</b> |
| <b>5</b> | <b>Comparison of the original softcore and SSC(2) functions with different values of <math>\alpha</math> and <math>\beta</math>:</b> | <b>S13</b> |
| <b>6</b> | <b>Results of smoothstep functions with different orders:</b>  | <b>S15</b> |

## 1 The direct space implementation of the electrostatic interaction

In the PME implementation of treatment of periodic electrostatic interactions, while the reciprocal contribution takes care of the long range periodic part through Gaussian screen charge distributions, the short-range, i.e., within the non-bonded cutoff, direct space contribution is usually written as

$$U_{dir}^C = \frac{1}{4\pi\epsilon_0} \operatorname{erfc}(\kappa r_{ij}) \frac{q_i q_j}{r_{ij}} = \frac{1}{4\pi\epsilon_0} [1 - \operatorname{erf}(\kappa r_{ij})] \frac{q_i q_j}{r_{ij}} \quad (1)$$

where  $q_i$ ,  $q_j$  are the particle charges,  $r_{ij}$  is the inter-particle distance, and  $\kappa$  is the PME coefficient, and the first part of the equation,  $\frac{q_i q_j}{r_{ij}}$ , is the Coulombic term and the second

term  $-\text{erf}(\kappa r_{ij}) \frac{q_i q_j}{r_{ij}}$  is the correction of the PME contribution. The current AMBER employs the soft-core potential by defining  $r_{ij}^{SC}$  to replace  $r_{ij}$  as

$$r_{ij}^{SC} \equiv (r_{ij}^2 + \lambda\beta)^{\frac{1}{2}} \quad (2)$$

and the direct space term is modified by the softcore potential as

$$U_{dir,sc}^C = \frac{1}{4\pi\epsilon_0} [1 - \text{erf}(\kappa r_{ij})] \frac{q_i q_j}{r_{ij}^{SC}} \quad (3)$$

In the current softcore implementation, only this direct space term  $U_{dir,sc}^C$  is relevant and usually the focus is only on  $\frac{q_i q_j}{r_{ij}^{SC}}$ , as in the main text. Furthermore,  $U_{dir,sc}^C$  is regulated by the quick declining  $[1 - \text{erf}(\kappa r_{ij})]$  term that is numerically very small at the cutoff boundary in the PME implementation through a proper choice of  $\kappa$ . As a result,  $U_{dir,sc}^C$  does not have significant discontinuity at the cutoff boundary even with a large  $\beta$ . To confirm, we performed simulations for  $\text{Na}^+ \rightarrow 0$  with single precision model (SPFP) and the NVE ensemble at  $\lambda = 0.5$  under different conditions. The energy drift in units of kcal/mol/DOF/ns (where DOF are the number of dynamical degrees of freedom) from 5-ns simulations, shown in Figure S1, are: plain MD (real state endpoint):  $4.7 \times 10^{-5}$ ; original softcore with  $\alpha=0.5$ ,  $\beta=12\text{\AA}^2$ :  $6.7 \times 10^{-5}$ ; SSC(2) with  $\alpha=0.2$ ,  $\beta=12\text{\AA}^2$ :  $6.2 \times 10^{-5}$ ; SSC(2) with  $\alpha=0.2$ ,  $\beta=50\text{\AA}^2$ :  $4.6 \times 10^{-5}$ . These results are comparable to those reported in other work,<sup>S1</sup> and also from MD simulation of the real state endpoint (plain MD above), and indicate that the SSC(2) scheme does not exacerbate energy drift relative to regular GPU-accelerated MD.

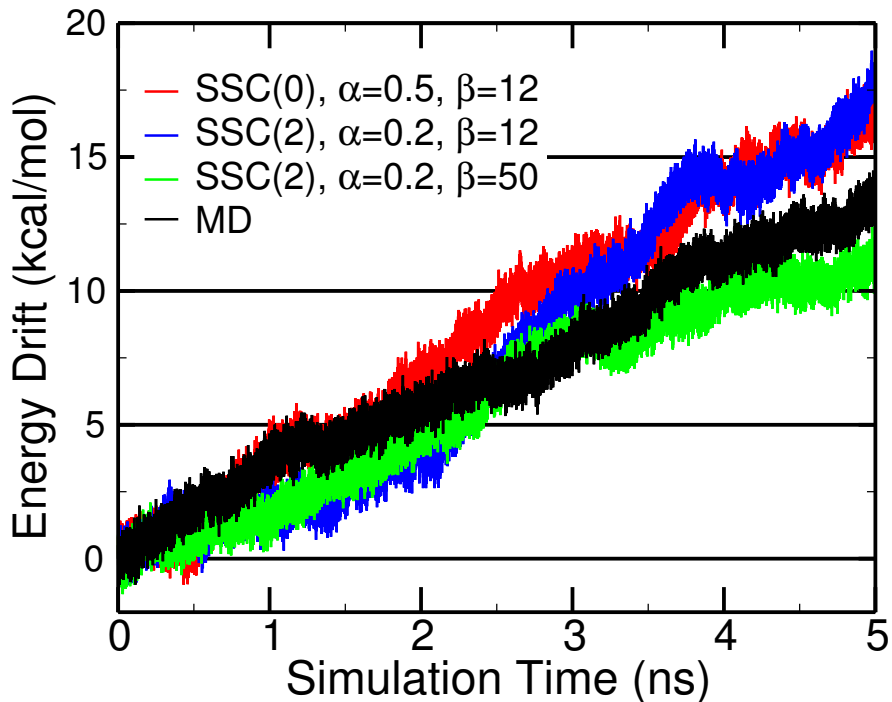


**Figure S1:** The potential energy drift in the absolute hydration calculations for  $\text{Na}^+ \rightarrow 0$  with single precision model (SPFP) and the NVE ensemble at  $\lambda = 0.5$  under different conditions. The energy drifts (in unit of kcal/mol/DOF/ns) from 5-ns simulations are: plain MD (real state endpoint):  $4.7 \times 10^{-5}$ ; original softcore with  $\alpha=0.5$ ,  $\beta=12 \text{ \AA}^2$ :  $6.7 \times 10^{-5}$ ; SSC(2) with  $\alpha=0.2$ ,  $\beta=12 \text{ \AA}^2$ :  $6.2 \times 10^{-5}$ ; SSC(2) with  $\alpha=0.2$ ,  $\beta=50 \text{ \AA}^2$ :  $4.6 \times 10^{-5}$ .

## 2 Simulation setup and protocols

A modified version of AMBER18 with the proposed SSC(P) scheme implementation, to be incorporated into AMBER20,<sup>S2</sup> was employed for all simulations. All simulations were performed with the recently implemented GPU-TI modules<sup>S3,S4</sup> built against the CUDA 10.1 GPU library and run on various GPU workstations and servers equipped with NVIDIA GTX 1080TI, RTX 2080 TI, Titan V, and V100 GPUs. Results reported here were created with single precision calculation/flexible precision accumulation (SPFP) model.<sup>S1</sup>

## 2.1 Three representative model systems

Three model alchemical transformations were selected: the absolute hydration free energies for diphenyl toluene (denoted as DPT/0 in the main text) and single  $\text{Na}^+$  ion ( $\text{Na}^+/0$ ), and the relative solvation free energy simulations for the Fact Xa ligand L51c to L51h mutation (denoted as L51c/h; the details of these ligands are described elsewhere.<sup>S5</sup>).

For DPT/0 and L51c/h, the atom types of the solute were assigned from General AMBER Force Field (GAFF, Version 1.8),<sup>S6</sup> Atomic partial charges were prepared using the AM1-BCC approach.<sup>S7,S8</sup> For  $\text{Na}^+/0$ , the AMBER default  $\text{Na}^+$  parameter of ff14SB<sup>S9</sup> is used. The initial structures of all three systems were prepared by putting the solvent molecule into a water box extending at least 11 Å in each direction, filled with pre-equilibrated TIP3P waters.<sup>S10</sup>

*Simulation protocols* As suggested,<sup>S11</sup> a time step of 1 fs was used for the integration of the equations of motion, since SHAKE<sup>S12</sup> is not employed in those mutation simulations involving deleting/adding hydrogens. The translational center-of-mass motion was removed every 1000 steps. Long-range electrostatic interactions were treated by the particle-mesh Ewald method (PME)<sup>S13,S14</sup> with a direct-space sum cutoff of 10 Å. The Ewald error tolerance is set to  $10^{-5}$  and the Ewald coefficient is automatically set according to the error tolerance. The FFT grid sizes are determined automatically by the AMBER program and are roughly 36-40 for the systems reported here.

*Setup/pre-equilibration for TI calculations* The parmed module of AMBER18 was used to prepare the topology files for TI calculations. The system for each mutation was first minimized and relaxed at 300 K in the NVT ensemble, then the initial conformations for each  $\lambda$  window were sequentially generated with 10 ps pre-equilibration for each  $\lambda$ -value from 0.0 to 1.0 with  $\Delta\lambda = 0.01$  (total 101 windows), where the final conformation of the current  $\lambda$  window was used as the starting conformation of the next  $\lambda$  window for a 50 ps production run. Note the high number of  $\lambda$ -windows is chosen in order to monitor the  $\langle dU/d\lambda \rangle_\lambda$  vs.  $\lambda$  behavior across the entire  $\lambda$  range as the purpose here is not to obtain accurate free energies.

## 2.2 Hydration free energies

Absolute and relative hydration energies are computed on the following small organic molecules: methane, ethane, methanol, toluene, neopentane, 2-methylfuran, 2-methylindole, 2-cyclopentanylindole (2-CPI) and 7-cyclopentanylindole (7-CPI). As for the methane→neopentane transformation, two mapping methods, terminally mapped and centrally mapped, have been considered. Terminally mapped has methane matched to terminal methyl group, while centrally mapped has the carbon of methane matched to the central carbon of neopentane. The initial structures were taken from the published data.<sup>S15</sup> The AMBER ff14SB<sup>S9</sup> and GAFF (Version 1.8)<sup>S6</sup> force fields were employed along with the AM1-BCC charges,<sup>S7,S8</sup> computed by the antechamber module in the AMBER program. The missing bonded and vdW terms are generated with parmchk2 module. The system is then solvated with TIP3P water molecules<sup>S10</sup> extending to 12 Å from the ligand. Initial structures for gaseous simulations are prepared by stripping water from those in the aqueous phase with periodic box. The production simulations are run with the constant temperature and constant volume ensemble (NVT). The temperature was controlled at 298 K through Langevin thermostat with a friction constant of 5.0 ps<sup>-1</sup>. A 1 fs timestep is used without constraint applied on the solute molecules. Nonbonded interactions are computed within a 10 Å cutoff and the electrostatics is handled with PME.<sup>S13,S14</sup> The system of each transformation are minimized and followed by a 500 ps equilibration for each  $\lambda$ -value from 0.0 to 1.0 with a spacing  $\Delta\lambda = 0.05$  (total 21 windows). The reported analysis results for every transformation are from 8 independent runs (21  $\lambda$  values for each run and each window simulated for 2.7 ns, with the first 200 ps discarded and 2.5 ns analyzed).

## 2.3 The Wang, *et al.* dataset

Initial structures were taken from the published data<sup>S16</sup> and simulations were prepared using the AMBER ff14SB,<sup>S9</sup> GAFF2<sup>S6</sup> force fields, and the TIP3P water model<sup>S10</sup> (including the associated alkaline and halide ion models). Ligands and ligand-protein complexes were

solvated in a truncated octahedron using AMBER18’s `t1eap` module and an initial buffer size of 12 and 8 Å, respectively. Any remaining net charge of the system was neutralized by addition of  $\text{K}^+$  or  $\text{Cl}^-$  ions as appropriate. During equilibration Cartesian restraints relative to the starting structure were applied to all ligand (and protein) heavy atoms (force constant of 5 kcal/mol-Å<sup>2</sup>). After a brief minimization (50 steps of steepest descent plus 450 steps of conjugate gradient), the system was sequentially heated at a fixed volume with a linear ramp between 5, 100, 200, and 298 K (20 ps per ramp followed by an additional 20 ps with pressure coupling). The restraints were then reduced to zero in 4 steps over 0.5 ns for solvated ligands and 1 ns for complexes. Finally, the resulting structures were converted to alchemical topologies by mapping the ligand atoms to a new ligand via a maximum common substructure algorithm. At this stage, the hydrogen masses were also increased to a target mass of 3.024 amu by repartitioning mass from the nearest bound heavy atom to allow a large time step.<sup>S17</sup> The heating steps were then repeated at each alchemical coupling value followed by production with no restraints (the first 20 ps is ignored as equilibration).

All simulations used a Langevin integrator with a 2 fs timestep for preparation and 4 fs for production, and a friction coefficient of 2 ps<sup>-1</sup>. With the exception of simulations involving a change in the temperature that were performed under constant volume conditions, pressure coupling was performed at 1 atm via a Monte Carlo barostat. Bonds to hydrogens were constrained via SHAKE,<sup>S12,S18</sup> except when both atoms reside in a softcore region. The standard AMBER protocol for non-bonded interactions was followed (PME.<sup>S13,S14</sup> electrostatics with an 8 Å direct space cutoff and hard truncation of Lennard-Jones interactions plus a long-range continuum correction on the dispersion term.<sup>S19</sup>).

Although neglecting specific SHAKE constraints is not necessarily ideal, in tests this did not lead to results that were discernible from using a 1 fs timestep (and the same simulation length). For five repeats of a perturbation from the p38 set the two step sizes yield differences of  $-0.40 \pm 0.74$  and  $-0.06 \pm 0.58$  kcal/mol for the stepwise and one-step schemes, respectively. Although the two alchemical pathways do not yield exactly identical results (difference of

$\sim 0.5$  kcal/mol) the difference remains for both timesteps, indicating that it is not caused from unseen integrator errors.

### 3 Representative $\langle \frac{\partial U}{\partial \lambda} \rangle_\lambda$ curves

#### **Problematic cases when using the original AMBER softcore scheme:**

In Figure S2 we demonstrate three problematic cases when using the concerted protocol with the original AMBER softcore scheme. These cases are representative of other problematic cases encountered throughout the dataset. The first case is 3fn $\rightarrow$ 2o in the p38 protein environment, the second 23482 $\rightarrow$  23479 in the PTP1B protein environment, and the third MCL1 ligand 28 $\rightarrow$  47 in water. The main reason of the very large standard deviations is the particle collapse problems around  $\lambda = 0.2$  and/or  $\lambda = 0.8$  to 0.9.

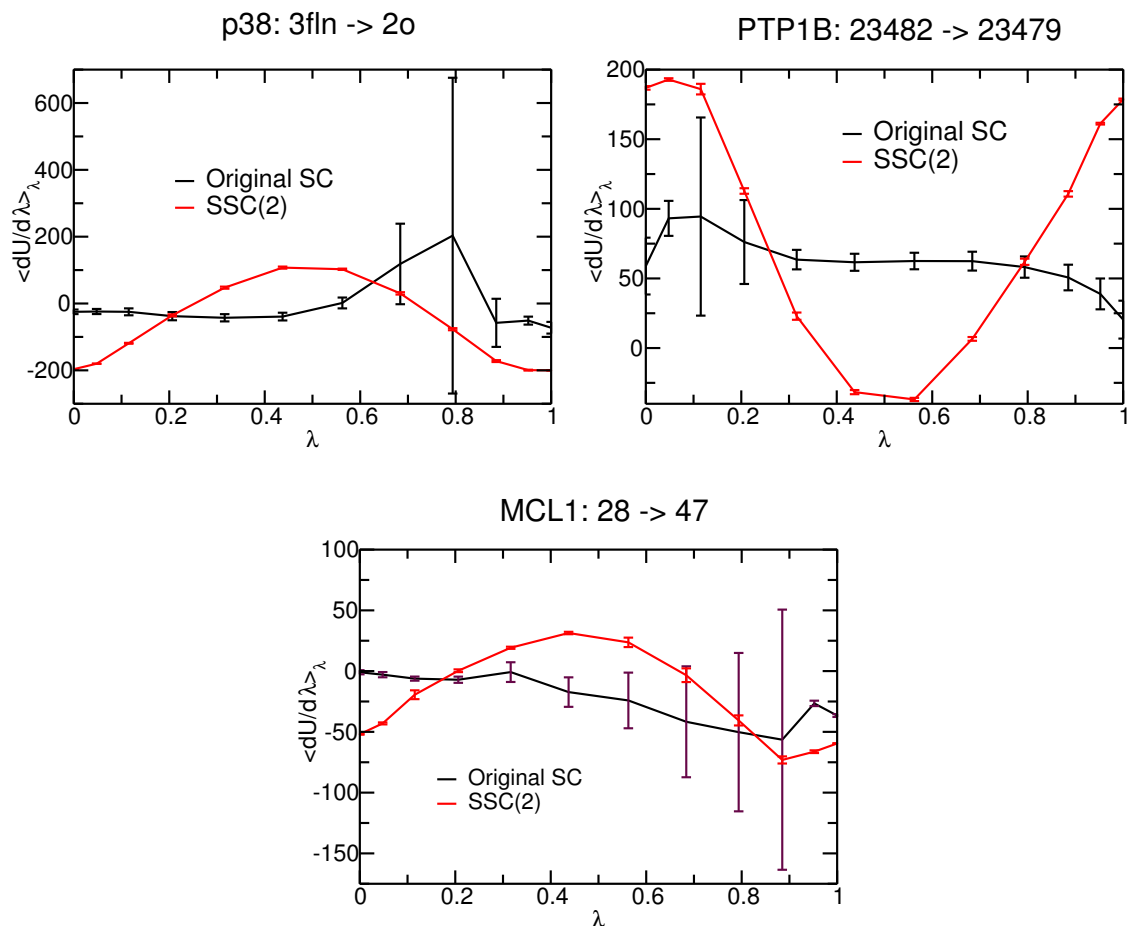


**Figure S2:** Three problematic  $\langle \frac{\partial U}{\partial \lambda} \rangle_\lambda$  curves (in black) resulted from the original AMBER softcore scheme. The first two are for the calculations of mutations in the protein environments while the last one is in water, and the mutations are labeled on the figures. The curves show the huge standard deviations around  $\lambda = 0.8$  for 3fln $\rightarrow$ 2o in in the p38 protein environment, around  $\lambda = 0.1 - 0.2$  for 23482 $\rightarrow$  23479 in the PTP1B protein environment, and around  $\lambda = 0.8 - 0.9$  for MCL1 ligand 28 $\rightarrow$  47 in water. The error bars indicate the corresponding standard deviations. The SSC(2) results are shown in red for comparison.

### Cases with slightly larger standard deviations:

In almost all cases reported in this study, the SSC(2) concerted scheme gives similar standard deviations compared to the stepwise scheme. Nevertheless, Figure S3 shows a case (the mutation of Tyk2 ligand ejm50  $\rightarrow$  ejm42 in water) where the SSC(2) scheme delivers larger standard deviation in  $\Delta G$  (0.75) compared to the original AMBER softcore scheme (0.14). Although the overall  $\Delta\Delta G$  is comparable and only differs by 0.11 kcal/mol (0.62 from

the SSC(2) concerted scheme; 0.51 from the stepwise scheme) and the error bars are also comparable in both schemes most of time, the relatively large standard deviations around  $\lambda = 0.1 - 0.3$  probably indicates that in such cases the particle collapse problems are still not completely solved and maybe more fine-tuned  $\alpha$  and  $\beta$  are needed for certain systems.

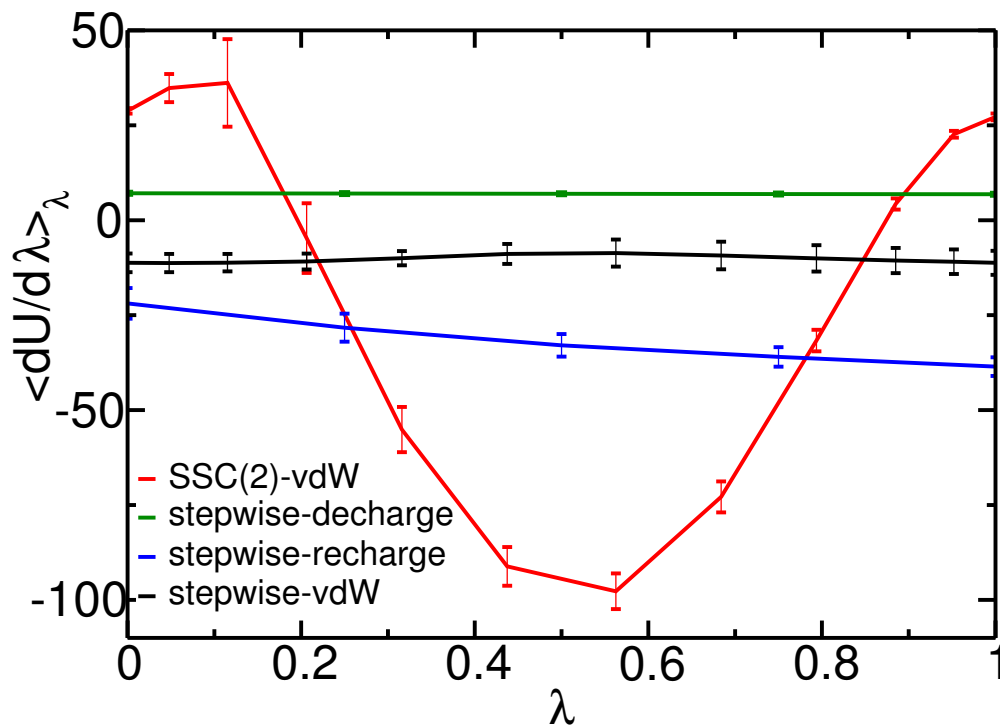


**Figure S3:** A case (the mutation of Tyk2 ligand  $\text{ejm50} \rightarrow \text{ejm42}$  in water) where the SSC(2) concerted scheme delivers larger standard deviation in  $\Delta G$  (0.75) compared to the stepwise scheme (0.14). The error bars indicate the corresponding standard deviations.

## 4 The smooth step functions of different orders and their derivatives:

The family of smoothstep functions of orders  $P$  ( $P = 0, 1, 2, \dots$ ) and are defined as the polynomial functions (up to  $P = 4$  shown):

for  $0 \leq x \leq 1$  :

$$S_0(x) = x,$$

$$S_1(x) = -2x^3 + 3x^2,$$

$$S_2(x) = 6x^5 - 15x^4 + 10x^3,$$

$$S_3(x) = -20x^7 + 70x^6 - 84x^5 + 35x^4,$$

$$S_4(x) = 70x^9 - 315x^8 + 540x^7 - 420x^6 + 126x^5,$$

and

$$S_P(x < 0) = 0; S_P(x > 1) = 1, \forall P \in \mathbb{N} \quad (4)$$

The smoothstep functions are monotonically increasing functions that have the desirable endpoint values:

$$S_P(0) = 0; S_P(1) = 1 \quad \forall P \in \mathbb{N} \quad (5)$$

and derivative properties

$$\left[ \frac{d^k S_P(x)}{dx^k} \right]_{x=0} = \left[ \frac{d^k S_P(x)}{dx^k} \right]_{x=1} = 0 \quad \forall k \in \mathbb{N}, \quad 0 < k \leq P \quad (6)$$

A smoothstep function with a higher order will have a smoother function curve and smaller derivatives near 0 and 1 but a larger derivative in between. The function values and the derivatives of the first few smoothstep functions are plot in Figure S4.

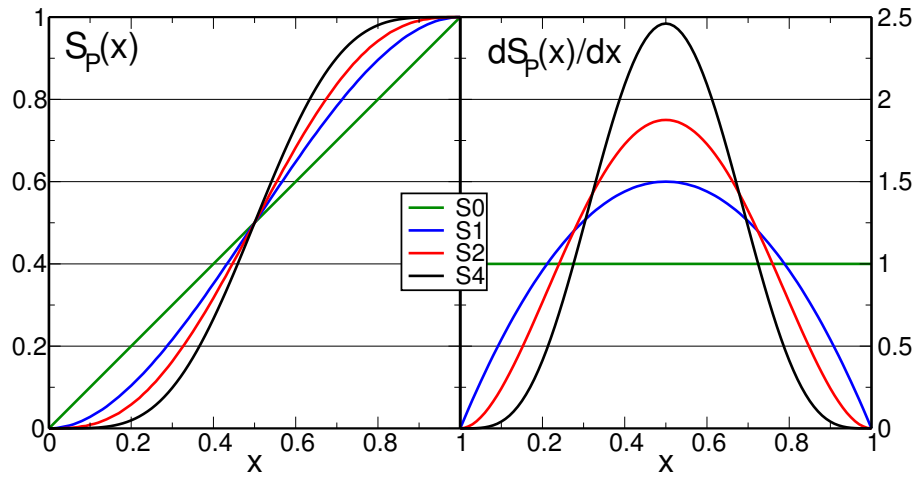


**Figure S4:** The function values (left) and derivatives (right) of the first five smoothstep functions. Note that a smoothstep function with a higher order will have a smoother function curve and smaller derivatives near 0 and 1 but a larger derivative in between.

## 5 Comparison of the original softcore and SSC(2) functions with different values of $\alpha$ and $\beta$ :

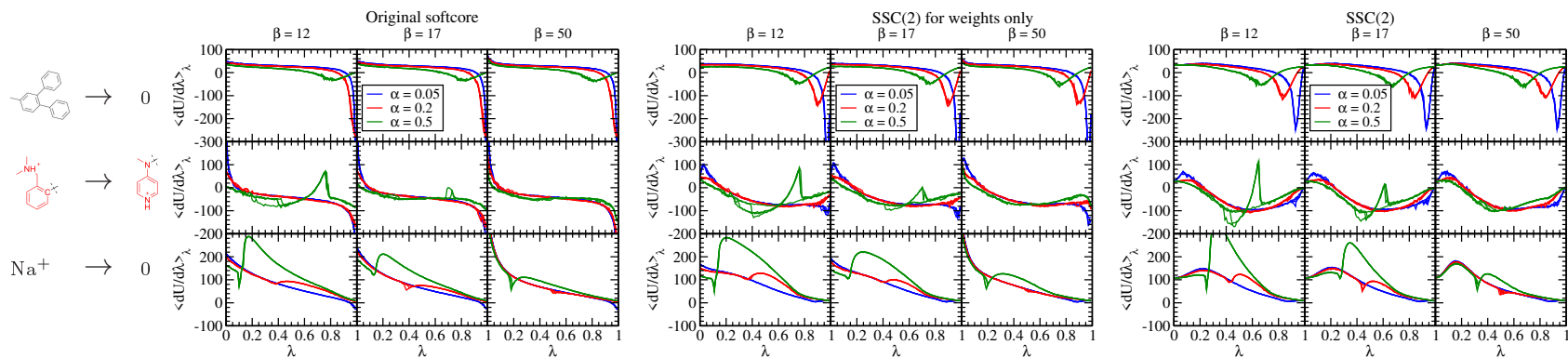


**Figure S5:** The  $\langle \partial U / \partial \lambda \rangle_\lambda$  vs.  $\lambda$  plots for alchemical simulations of three molecular systems shown on the left (and identical to those shown in Figure 1 in the main text) using a concerted pathway with different softcore potentials. The leftmost set is for the original softcore potential, which is the same as the SSC(0) potential and identical to the colored curves shown in Figure 1 in the main text, using different parameters. Note that this softcore potential has linear *lambda* dependence in the weights for the  $U_0^{SC}$  and  $U_1^{SC}$  potentials in Eqn. 4. The rightmost set is for the SSC(2) smoothstep softcore potential as presented in the manuscript using different variations of  $\alpha$  and  $\beta$  parameters. Note that this potential includes the smoothstep function both in the weights for the  $U_0^{SC}$  and  $U_1^{SC}$  potentials of Eqn. 23 of the main text, but also as  $\lambda$  arguments to the functions in Eqn. 4 of the main text, i.e.,  $U_0^{SC}[\mathbf{q}, S_2(\lambda)]$  and  $U_1^{SC}[\mathbf{q}, 1 - S_2(\lambda)]$  in Eqn. 23. The middle set (labeled “SSC(2) for weights only”) is identical to the original method (leftmost set) but instead of using linear weights, the SSC(2) potential is used for the  $U_0^{SC}$  and  $U_1^{SC}$  potentials. This is done to decompose the SSC(2) potential into components for illustrative purposes. It is clear that, not matter which form of the softcore potential is used, the  $\alpha$  and  $\beta$  parameters need to be balanced in order to produce stable results. For properly balanced parameters, the use of SSC(2) potential for non-linear weights (middle set) improves the behavior, but large values persist at the endpoints that are not eliminated unless the full SSC(2) potential is used. With SSC(2) and  $\alpha=0.2$  and  $\beta=50 \text{ \AA}^2$ , all three cases have smooth  $\langle \partial U / \partial \lambda \rangle_\lambda$  vs.  $\lambda$  curves in the entire range between  $\lambda=0$  and 1.

Figure S6 below shows the interaction potential between a  $\text{Na}^+$  ion with a TIP3P water oxygen for the original AMBER18 softcore potential and the smoothstep softcore potential developed in the current work. It should be kept in mind this 2-particle system is meant to be an exaggerated example for illustrative purposes. This otherwise is an artificial extreme case in the sense that these interactions neglect the positively charged hydrogens on the water and would further be highly screened in solution. With the original softcore potential, there are deep minima at the origin for even small  $\lambda$  values, which would exacerbate the particle collapse problem. The smoothstep softcore potential, on the other hand, remains repulsive for small  $\lambda$  values, and has considerably reduced minima at the origin. Hence, as discussed in the paper, the current smoothstep softcore potential is expected to improve the particle collapse problem, but does not guarantee that artificial minima will not occur at intermediate  $\lambda$  values for some edge cases. As the smoothstep softcore potential is further tested and new data is considered, further exploration of the form of the softcore potential and optimization of parameters therein may lead to even more stable and robust concerted alchemical pathways. In this sense, it is the hope that the smoothstep softcore potential introduced here is a valuable step forward.

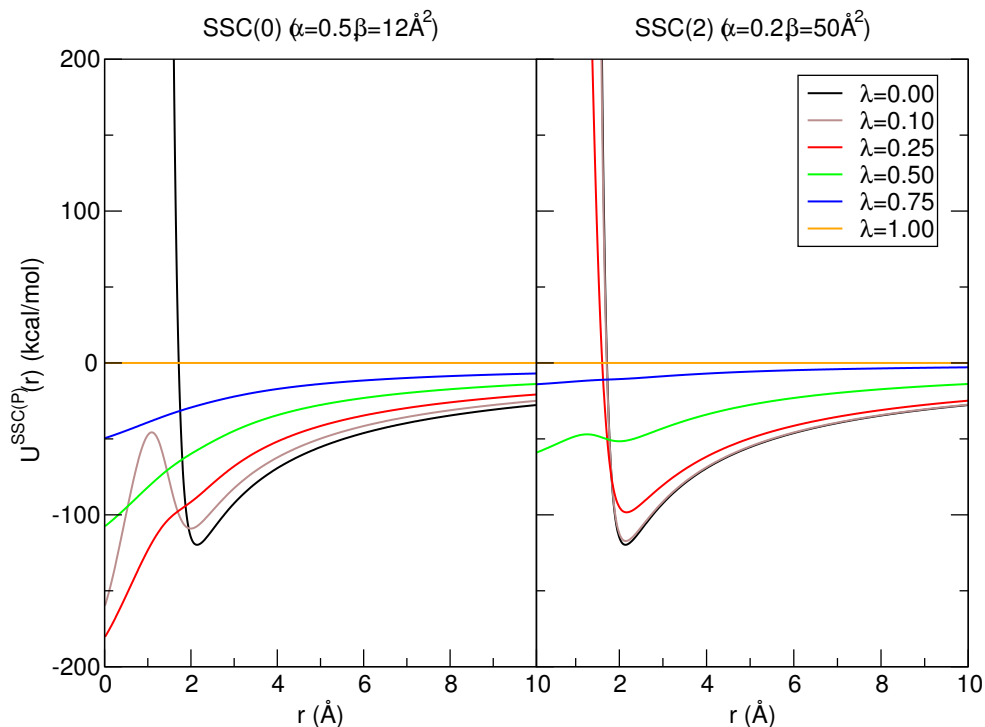


**Figure S6:** Illustration of the  $U^{SSC(P)}$  potential for the interaction of a  $\text{Na}^+$  ion with a TIP3P water oxygen as a function of separation distance,  $r$ , for various values of  $\lambda$  ( $\lambda=0$  and 1 represent the real and non-interacting dummy states, respectively). The SSC(0) softcore potential is the original softcore potential in AMBER18 with default  $\alpha$  and  $\beta$  parameters. The SSC(2) smoothstep softcore potential is the default in AMBER20 with default parameters developed in the current work.

## 6 Results of smoothstep functions with different orders:

Figures S7 to S9 below show the  $\langle dU/d\lambda \rangle_\lambda$  vs.  $\lambda$  curves for alchemical simulations of three molecular systems using the one-step unified scheme with various conditions mentioned in the main text, including the absolute solvation free energies for diphenyl toluene (upper panels) and single  $\text{Na}^+$  ion (lower panels), and the relative solvation free energy simulations for the Fact Xa ligand L51c to L51h mutation (middle panels). The SSC(2) results are already shown in the main text and the SSC(1) and SSC(4) results here demonstrate that all three smoothstep functions are capable to solve the problems as expected.

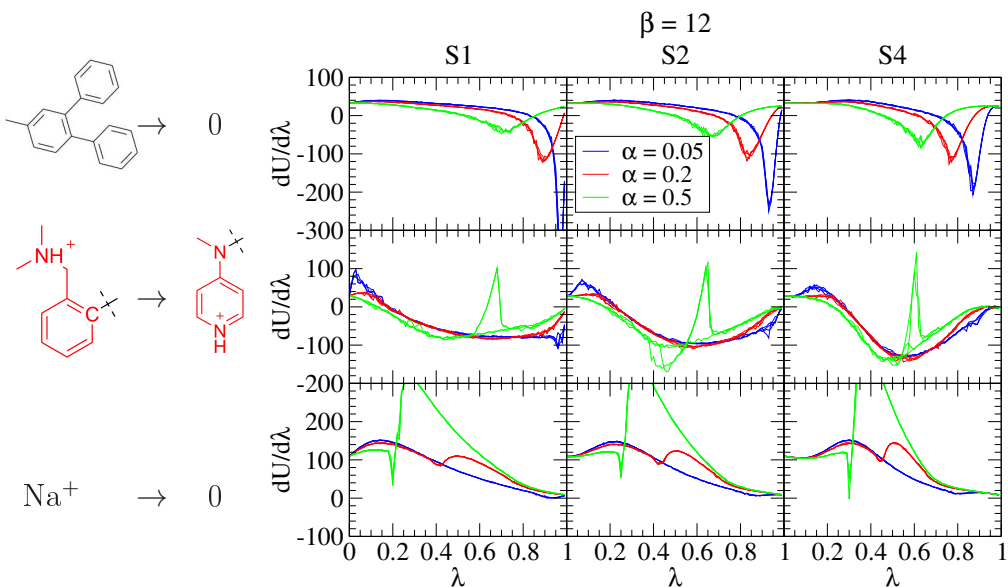


**Figure S7:** The  $\langle \partial U / \partial \lambda \rangle_\lambda$  vs.  $\lambda$  plots for alchemical simulations of three molecular systems using the one-step unified scheme: the absolute solvation free energies for diphenyl toluene (upper panels) and single  $\text{Na}^+$  ion (lower panels), and the relative solvation free energy simulations for the Fact Xa ligand L51c to L51h mutation (middle panels). The L51c ligand has 65 atoms and L51h 58 atoms. The red-colored atoms shown are the defined softcore regions, i.e., the unique atoms for the individual ligands. The atoms common to both ligand are not shown except the connecting carbon shown in black. The three columns correspond to the smooth functions of different orders (1,2, and 4), and different colored curves correspond to different  $\alpha$  values. Each curve represents one 101-window (total 5 ns) TI simulation and there are four simulations for each condition. This figure show the results of  $\beta = 12 \text{ \AA}^2$ .

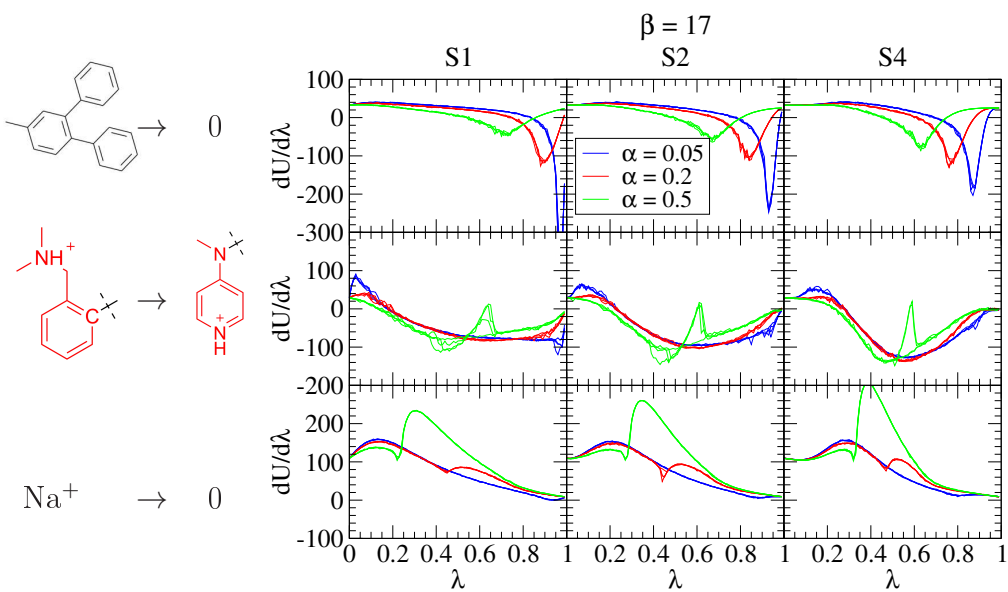


**Figure S8:** The same figure as Figure S7, except this figure show the results of  $\beta = 17 \text{ \AA}^2$ .

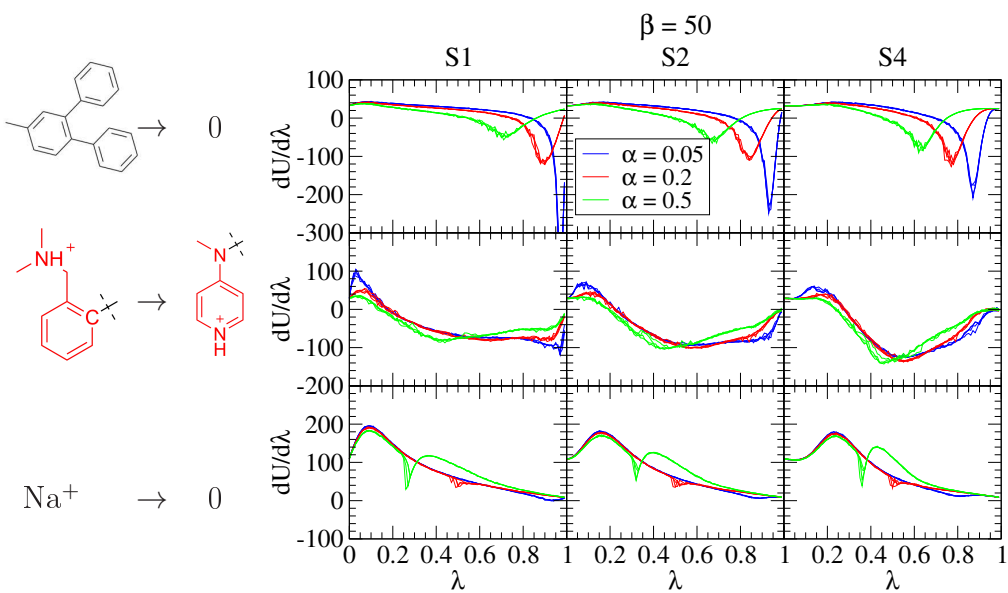


**Figure S9:** The same figure as Figure S7, except this figure show the results of  $\beta = 50 \text{ \AA}^2$ .

## References

- (S1) Le Grand, S.; Göetz, A. W.; Walker, R. C. *Comput. Phys. Commun.* **2013**, *184*, 374–380.
- (S2) Case, D. A.; Belfon, K.; Ben-Shalom, I. Y.; Brozell, S. R.; Cerutti, D. S.; Cheatham III, T. E.; Cruzeiro, V. W. D.; Darden, T. A.; Duke, R. E.; Giambasu, G.; Gilson, M. K.; Gohlke, H.; Goetz, A. W.; Harris, R.; Izadi, S.; Izmailov, S. A.; Kasavajhala, K.; Kovalenko, K.; Krasny, R.; Kurtzman, T.; Lee, T.; Le-Grand, S.; Li, P.; Lin, C.; Liu, J.; Luchko, T.; Luo, R.; Man, V.; Merz, K.; Miao, Y.; Mikhailovskii, O.; Monard, G.; Nguyen, H.; Onufriev, A.; Pan, F.; Pantano, S.; Qi, R.; Roe, D. R.; Roitberg, A.; Sagui, C.; Schott-Verdugo, S.; Shen, J.; Simmerling, C. L.; Skrynnikov, N.; Smith, J.; Swails, J.; Walker, R. C.; Wang, J.; Wilson, R. M.; Wolf, R. M.; Wu, X.; Xiong, Y.; Xue, Y.; York, D. M.; Kollman, P. A. AMBER 20. University of California, San Francisco: San Francisco, CA, 2020.
- (S3) Lee, T.-S.; Cerutti, D. S.; Mermelstein, D.; Lin, C.; LeGrand, S.; Giese, T. J.; Roitberg, A.; Case, D. A.; Walker, R. C.; York, D. M. *J. Chem. Inf. Model.* **2018**, *58*, 2043–2050.
- (S4) Lee, T.-S.; Hu, Y.; Sherborne, B.; Guo, Z.; York, D. M. *J. Chem. Theory Comput.* **2017**, *13*, 3077–3084.
- (S5) Hu, Y.; Sherborne, B.; Lee, T.-S.; Case, D. A.; York, D. M.; Guo, Z. *J. Comput.-Aided Mol. Des.* **2016**, *30*, 533–539.
- (S6) Wang, J.; Wolf, R. M.; Caldwell, J. W.; Kollman, P. A.; Case, D. A. *J. Comput. Chem.* **2004**, *25*, 1157–1174.
- (S7) Jakalian, A.; Jack, D. B.; Bayly, C. I. *J. Comput. Chem.* **2002**, *23*, 1623–1641.

- (S8) Jakalian, A.; Bush, B. L.; Jack, D. B.; Bayly, C. I. *J. Comput. Chem.* **2000**, *21*, 132–146.
- (S9) Maier, J. A.; Martinez, C.; Kasavajhala, K.; Wickstrom, L.; Hauser, K. E.; Simmerling, C. *J. Chem. Theory Comput.* **2015**, *11*, 3696–3713.
- (S10) Jorgensen, W. L.; Chandrasekhar, J.; Madura, J. D.; Impey, R. W.; Klein, M. L. *J. Chem. Phys.* **1983**, *79*, 926–935.
- (S11) Case, D.; Babin, V.; Berryman, J.; Betz, R.; Cai, Q.; Cerutti, D.; Cheatham III, T.; Darden, T.; Duke, R.; Gohlke, H.; Goetz, A.; Gusarov, S.; Homeyer, N.; Janowski, P.; Kaus, J.; Kolossváry, I.; Kovalenko, A.; Lee, T.; LeGrand, S.; Luchko, T.; Luo, R.; Madej, B.; Merz, K.; Paesani, F.; Roe, D.; Roitberg, A.; Sagui, C.; Salomon-Ferrer, R.; Seabra, G.; Simmerling, C.; Smith, W.; Swails, J.; Walker, R.; Wang, J.; Wolf, R.; Wu, X.; Kollman, P. *AMBER 14*; University of California, San Francisco: San Francisco, CA, 2014.
- (S12) Ryckaert, J. P.; Ciccotti, G.; Berendsen, H. J. C. *J. Comput. Phys.* **1977**, *23*, 327–341.
- (S13) Darden, T.; York, D.; Pedersen, L. *J. Chem. Phys.* **1993**, *98*, 10089–10092.
- (S14) York, D. M.; Wlodawer, A.; Pedersen, L. G.; Darden, T. *Proc. Natl. Acad. Sci. USA* **1994**, *91*, 8715–8718.
- (S15) Loeffler, H. H.; Bosisio, S.; Duarte Ramos Matos, G.; Suh, D.; Roux, B.; Mobley, D. L.; Michel, J. *J. Chem. Theory Comput.* **2018**, *14*, 5567–5582.
- (S16) Wang, L.; Wu, Y.; Deng, Y.; Kim, B.; Pierce, L.; Krilov, G.; Lupyan, D.; Robinson, S.; Dahlgren, M. K.; Greenwood, J.; Romero, D. L.; Masse, C.; Knight, J. L.; Steinbrecher, T.; Beuming, T.; Damm, W.; Harder, E.; Sherman, W.; Brewer, M.; Wester, R.; Murcko, M.; Frye, L.; Farid, R.; Lin, T.; Mobley, D. L.; Jorgensen, W. L.; Berne, B. J.; Friesner, R. A.; Abel, R. *J. Am. Chem. Soc.* **2015**, *137*, 2695–2703.

- (S17) Hopkins, C. W.; Le Grand, S.; Walker, R. C.; Roitberg, A. E. *J. Chem. Theory Comput.* **2015**, *11*, 1864–1874.
- (S18) Miyamoto, S.; Kollman, P. A. *J. Comput. Chem.* **1992**, *13*, 952–962.
- (S19) in't Veld, P. j.; Ismail, A. E.; Grest, G. S. *J. Chem. Phys.* **2007**, *127*, 144711.